Quaternary Science Reviews 313 (2023) 108192

Contents lists available at ScienceDirect

Quaternary Science Reviews

journal homepage: www.elsevier.com/locate/quascirev

# A new deglacial climate and sea-level record from 20 to 8 ka from IODP381 site M0080, Alkyonides Gulf, eastern Mediterranean

Ilaria Mazzini [a, *], Thomas M. Cronin [b], Robert L. Gawthorpe [c], Richard E. Ll Collier [d], Gino de Gelder [e, f], Anna Rose Golub [b], Michael R. Toomey [b], Robert K. Poirier [b], Huai-Hsuan May Huang [g, h], Marcie Purkey Phillips [i], Lisa C. McNeill [j], Donna J. Shillington [k]

[a] CNR- Institute of Environmental Geology and Geoengineering, Area Della Ricerca di Roma 1, Via Salaria Km 29, 300, 00015, Montelibretti, RM, Italy
[b] Florence Bascom Geoscience Center, National Center, MS 926A, U.S. Geological Survey, 12201 Sunrise Valley Drive, Reston, VA, 20192, USA
[c] Department of Earth Science, University of Bergen, P.O. Box 7803, N-5020, Bergen, Norway
[d] School of Earth and Environment, The University of Leeds, Leeds, United Kingdom
[e] ISTerre, CNRS, IRD, Université Grenoble-Alpes, St. Martin d'Hères, France
[f] Res. Group of Paleoclimate & Paleoenvironment, Res. Centr. for Climate and Atmosphere, Res. Org. of Earth Sciences and Maritime, National Research and Innovation Agency, Bandung, Republic of Indonesia
[g] Department of Paleobiology, National Museum of Natural History, Smithsonian Institution, Washington, DC, 20013-7012, USA
[h] Department of Geosciences, Princeton University, Princeton, NJ, 08544, USA
[i] University of Texas Institute for Geophysics, Austin, TX, 78758, USA
[j] School of Ocean and Earth Science, University of Southampton, Southampton, SO14 3ZH, UK
[k] Northern Arizona University, School of Earth and Sustainability, Flagstaff, AZ, 86011, USA

## ARTICLE INFO

*Article history:*
Received 20 January 2023
Received in revised form
2 June 2023
Accepted 11 June 2023
Available online 30 June 2023

Handling Editor: I Hendy

*Keywords:*
Ostracodes
Termination 1
Paleoenvironmental reconstruction
Climate changes
Corinth basin

## ABSTRACT

Records of relative sea-level rise for the last deglaciation are mostly limited to coral reef records and geophysical model estimates, but observational data from regions with temperate climates is sparse. We present a new relative climatic and regional sea-level rise record for glacial Termination 1 (Marine Isotope Stages [MIS] 2–1) based on ostracode paleoecology from the upper 8 m of the International Ocean Discovery Program (IODP) Site M0080 collected on Expedition 381, in the Gulf of Alkyonides, eastern Corinth basin of the Mediterranean Sea. Results show a series of major faunal transitions from lacustrine (Ponto-Caspian, Lake Corinth) glacial-age assemblages to fully marine (Mediterranean) interglacial assemblages between 20 and 8 ka. During glacial and early deglacial intervals, the Gulf of Alkyonides was characterized by non-marine lacustrine conditions with episodic sediment input from coastal, saline lake environments. Relatively stable lake shoreline conditions marked by the distinctive *Tuberoloxoconcha* sp. Existed from ~17.5 to 15 ka. During the peak deglacial interval, the BØlling-AllerØd (B-A, ~15–13.5 ka), rapid sea-level rise is indicated by a fully marine ostracode fauna colonization, which persisted from 13.5 to 7.5 ka (Late Pleistocene-Early to Middle Holocene).

The transition from lacustrine to marine environments confirms that during the last glacial maximum (LGM) low sea level (130 - 125 m below present day), the Corinth-Alkyonides depocentres were lacustrine. Marine water breached the shallow Rion and Acheloos-Cape Pappas sills, which today are ~50–60 m deep, separating the Mediterranean and Corinth-Alkyonides system beginning about 15 ka. Based on Alkyonides sedimentation rates, mean rates of sea-level rise during the B-A flooding of the Corinth-Alkyonides system are comparable to those obtained from coral reef sea level (SL) records, at least 10–20 mm $yr^{-1}$. Changes in sedimentation and sill depths in this tectonically active region may have played a role in reconnection of the Mediterranean and Corinth/Alkyonides system over a prolonged period. However, the ages and scale of the faunal changes and their clear correspondence with previously published global sea-level curves and the regional sea-level curve based on deglacial land elevation

* Corresponding author.
*E-mail address:* ilaria.mazzini@cnr.it (I. Mazzini).

https://doi.org/10.1016/j.quascirev.2023.108192

changes predicted by the ICE-7G model suggests the M0080A deglacial is dominated by the glacio-eustatic sea-level rise and records details of global climate changes during Termination 1.



## 1. Introduction

During the late Quaternary, global sea level oscillated by up to ~125–130 m between glacial lowstands and interglacial highstands caused by large ice sheet growth and decay. These ice volume changes are linked to orbital-scale paleoclimate variations known from benthic foraminifera oxygen isotope records (e.g., Lisiecki and Raymo, 2005; Lisiecki and Raymo, 2009), when correcting for deep-sea bottom temperature changes (e.g., Lea et al., 2002; Waelbroeck et al., 2002; Elderfield et al., 2012), and can be tied to uranium-series dated coral reef terraces (Past Interglacials Working Group of PAGES, 2016). Sea-level rise during the last deglaciation, Termination I (~19–7 ka), has been documented mainly from coral reef and continental margin records summarized in Supplement Table 1 of Lambeck et al. (2014) and geophysical modeling of glacio-isostatic adjustment (GIA) (Lambeck et al., 2014; Peltier et al., 2015,2021; Roy and Peltier, 2018). However, additional regional sea-level records are required to test these global sea-level records and glacio-isostatically corrected regional sea-level models (e.g., Roy and Peltier, 2018). In 2017, IODP Expedition 381 recovered sediment core from Site M0080 (Latitude: 38.12000°N, Longitude: 23.08630°E, 348.8 m water depth) down to 534.1 m below seafloor (mbsf) from the Gulf of Alkyonides (McNeill et al., 2019a) (Fig. 1). The main objective was to examine rift stratigraphy and tectonic history of this region located in the eastern part of the Corinth rift system (McNeill et al., 2019b). The Corinth-Alkyonides Gulf also contains excellent sea level and paleoclimate records due to the well-defined cyclic nature of sedimentation in the system (e.g., Collier et al., 2000; Leeder et al., 2002) (Fig. 2), orbital-scale onshore and offshore sea-level records (e.g., de Gelder et al., 2019), and orbital records from the eastern Mediterranean (Konijnendijk et al., 2015). The Corinth-Alkyonides depocentres are partially closed in the west, across the Straits of Rion, by a sill which is currently 50–60 m below sea level. The Corinth and Alkyonides depocentres are themselves separated by a sill 320 m below sea level, in the hanging wall to the West Alkyonides Fault (Leeder et al., 2002). During glacio-eustatic lowstands, when the rift was occupied by a lake maintained at the level of the western sill, the Alkyonides depocentre remained a deep-water lake (Collier et al., 2000; Leeder et al., 2002, 2005; McNeill et al., 2019b). In such complex palaeoenvironmental settings, ostracodes can be particularly useful proxies, because, unlike other commonly used micropaleontological proxies such as foraminifera and nannoplankton, ostracodes occur in almost all aquatic environments, from deep marine to temporary freshwater. Consequently, core M0080 offers an opportunity to examine Quaternary glacial-interglacial sea-level oscillations in detail, specifically providing insights into the pattern of sea-level rise above the level of the Rion sill during Termination I, and to test our findings against other climatic records.

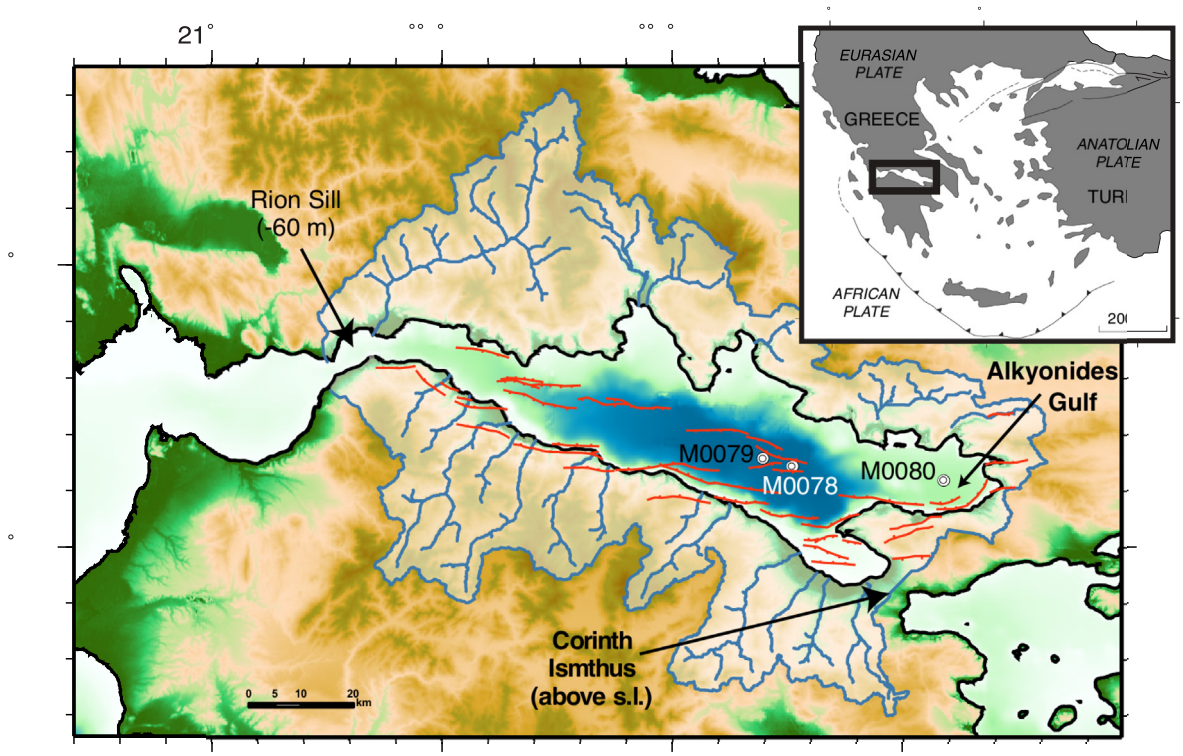


**Fig. 1.** A. Map showing Gulf of Corinth/Alkyonides bathymetry, and fault distribution and location of IODP Leg 381 sites (Nixon et al., 2016 and McNeill et al., 2019a). The current study focused on Site M0080 in the Gulf of Alkyonides.

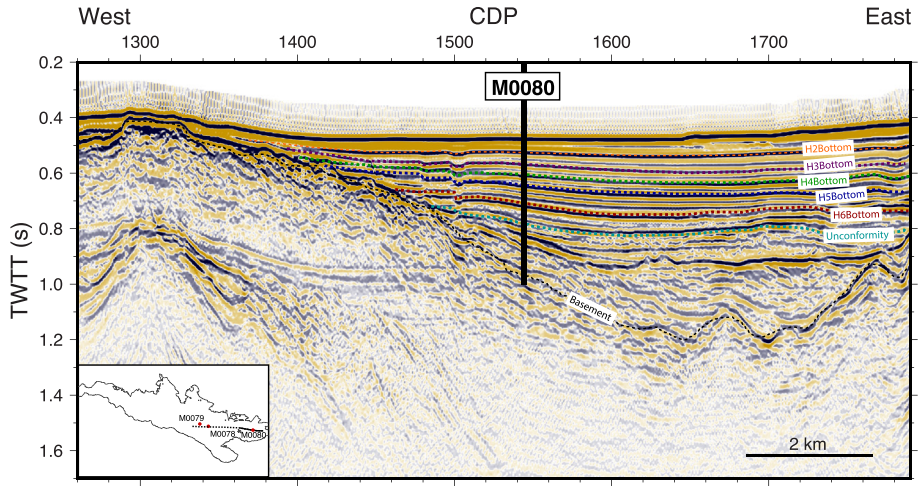


**Fig. 2.** Seismic stratigraphy for the Gulf of Alkyonides showing location of Site M0080. The seismic line is *Maurice Ewing* Line 22 (Taylor et al., 2011) and interpretations from Nixon et al. (2016)(colored dotted lines and text). CDP = common depth point, TWT = two-way traveltime. Inset: seismic line and drill site locations.

## 2. Materials & methods

Initially, samples from the upper 178 m of core were used for micropaleontological analyses of marine and non-marine ostracodes. Sample spacing of 0.5–3 m was guided by lithostratigraphy, depth to seismic reflectors H1 through H6 shown in Fig. 2 (Nixon et al., 2016) and shipboard analyses of marine intervals based on foraminifera and other microfaunal groups (McNeill et al., 2019b). This information guided higher frequency sampling every 10 cm or less from the interval 8 to 3 mbsf core depth, representing Termination 1, for radiocarbon dating and focused study of the marine transgression during the last deglaciation. The sediment samples came from the depth range 3 m–7.90 mbsf, corresponding to lithostratigraphic unit 1 (McNeill et al., 2019a). In particular, subunit 1 (0 m–6.24 mbsf) consists of olive gray homogeneous mud with sparse organic layers and subunit 1–2 (6.24 m–22.83 mbsf) characterized by alternations of greenish gray bedded mud and gray to black silty beds (McNeill et al., 2019a). Sediment was processed by first washing through a 63-μm sieve and drying in an oven. Ostracodes from the >125-μm size fraction were picked under a stereomicroscope. Ostracodes were abundant and well preserved in almost all samples. A total of 49 taxa were identified at the Consiglio Nazionale delle Ricerche, IGAG, Rome and the U. S. Geological Survey, Reston, Virginia using taxonomy and ecology from a large Mediterranean and Ponto-Caspian literature (given in Supplementary Appendix).

## 3. Results

### 3.1. Chronostratigraphy

Preliminary shipboard calcareous nannofossil data indicate that the interval from 0 to 6.24 mbsf represents the Holocene interglacial (MIS 1), the 8.87–21.15 mbsf section is roughly 70 ka, and 35.4 mbsf is dated as MIS 7 or younger (Purkey Phillips in McNeill et al., 2019b) confirming earlier studies of the Alkyonides stratigraphy (Collier et al., 2000). It should be noted that the occurrence of *Emiliani huxleyi* down to 35.45 m may not reflect its total range as its true appearance is during a glacial period when nannofossils are not preserved (in the non-marine intervals).

An age model for the deglacial interval of the Site M0080 core was developed from 6 benthic foraminifera and 4 non-marine ostracode radiocarbon dates from the National Ocean Sciences Accelerator Mass Spectrometry (NOSAMS) facility (Table 1), collected from the 7.85 to 3.70 mbsf interval. For each date 200–300 specimens were used, with a cumulative weight ranging from ~2 to 8.5 mg. Additionally, two dates representing the last glacial period were obtained from organic material recovered at core depths of 8.5 and 11.26 mbsf by the Poznan Radiocarbon Laboratory. Radiocarbon dates from foraminifera were calibrated using Intcal 2020(Reimer et al., 2020), with those from ostracodes (non-marine) being calibrated via CALIB 2020 (Stuiver et al., 2021). Using these ten radiocarbon dates, we computed a linear age-depth model yielding an inferred mean sedimentation rate of 27.1 cm/kyr (S-Fig. 1). A second age model incorporating four additional radiocarbon dates from mollusk fragments yielded a similar sedimentation rate (28.9 cm/kyr) but produced a lower $r^2$ value compared to the original age model (0.744 vs 0.927, respectively). These are most likely hemipelagic background rates for the marine interval but may represent sediment accumulation rates that include undifferentiated turbidite intervals. We chose to use the model using foraminifers and ostracodes only due to potential transport, reworking or vital effects on mollusk shells. We also computed an age model with the 10 dates using the Bacon age model (Blaauw and Christen, 2011, https://chrono.qub.ac.uk/blaauw/manualBacon_2.3.pdf), which generally produced very similar ages to the foram-ostracode model (Supplement Fig. S1). Although sedimentation rates in the Gulf of Alkyonides vary during glacial and interglacial periods due to tectonic and paleoclimate influences on sediment flux, our record suggests a mean sedimentation rate of about 35–37 cm/kyr for the last deglaciation and a sampling resolution of ~125 yr for the period of most rapid sea-level-rise (SLR), corresponding with the BØlling-AllerØd warming event. These high sedimentation rates and high sampling resolution allow us to capture the timing of important centennial to millennial changes in deglacial inundation rates.

### 3.2. Faunal assemblages and taphonomy

The sedimentation in the Corinth-Alkyonides system is complex, highly variable both spatially and temporally, and subject to mixing due to downslope transport, potentially introducing artifacts within micropaleontological faunas. The ostracod species are subdivided into ecological/environmental groups (OEG, Mazzini et al., 2017) depending on their autoecological characteristics and distribution patterns recorded across the Mediterranean and

**Table 1**
Summary of all the radiocarbon dates performed on different materials from core M0080.

| **Radiocarbon dates** | | | | | | | | | | |
|---|---|---|---|---|---|---|---|---|---|---|
| **Receipt #** | **Calib** | **MBSF** | **Material** | **14C-age** | **CMBSF** | **Age Err** | **δ13X** | **20-CalAge** | **95%** | |
| 165,009 * | MARINE 20 | 3.7 | Benthic forams | 7810 | 370 | 40 | −0.46 | 8090 | 7939 | 8255 |
| 165,011 * | MARINE 20 | 4.05 | Benthic forams | 9820 | 405 | 50 | −0.42 | 10,607 | 10,376 | 10,843 |
| 165,013 * | MARINE 20 | 5.15 | Benthic forams | 10,800 | 515 | 55 | −0.57 | 12,042 | 11,788 | 12,357 |
| 166,921 * | MARINE 20 | 5.32 | Benthic forams | 10,250 | 532 | 40 | −0.55 | 11,209 | 11,060 | 11,389 |
| 165,015 * | MARINE 20 | 5.7 | Benthic forams | 12,250 | 570 | 70 | −0.25 | 13,595 | 13,371 | 13,801 |
| 166,920 * | MARINE 20 | 5.82 | Benthic forams | 13,300 | 582 | 45 | 0.02 | 15,166 | 14,941 | 15,408 |
| 165,017 * | IntCal20 | 6.65 | Non-marine Ostracodes | 13,800 | 665 | 95 | −1.69 | 16,744 | 16,432 | 17,026 |
| 166,922 * | IntCal20 | 6.82 | Non-marine Ostracodes | 15,950 | 682 | 80 | −0.73 | 19,260 | 19,042 | 19,482 |
| 165,018 * | IntCal20 | 7.15 | Non-marine Ostracodes | 14,450 | 715 | 85 | 0.72 | 17,626 | 17,362 | 17,904 |
| 165,019 * | IntCal20 | 7.85 | Non-marine Ostracodes | 16,400 | 785 | 110 | 0.15 | 19,780 | 19,530 | 20,096 |
| Organic material (de Gelder) radiocarbon dates | | | | | | | | | | |
| 10,780 | | 8.5 | organic matter | 18,010 | 850 | 100 | | | | |
| 10,803 | | 11.26 | organic matter | 24,490 | 1126 | 170 | | | | |
| Delta R for MARINE 20 dates = 92 ± 55 years | | | | | | | | | | |
| *Ten dates used in linear and Bacon age models | | | | | | | | | | |
| **Mollusc dates not used in age model** | | | | | | | | | | |
| **Receipt #** | **Calib** | **MBSF** | **Material** | **14C-age** | **CMBSF** | **Age Err** | **δ13X** | **20-CalAge** | **95%** | |
| 165,010 | MARINE 20 | 4 | Mixed, molluc fragments | 11,200 | 400 | 65 | −0.65 | 12,569 | 12,382 | 12,729 |
| 165,012 | MARINE 20 | 4.65 | Benthics & mollusc fragments | 7100 | 465 | 35 | −0.32 | 7404 | 7267 | 7545 |
| 165,014 | MARINE 20 | 5.6 | Mollusc fragments & benthics | 9510 | 560 | 45 | −1.1 | 10,200 | 10,007 | 10,401 |
| 165,016 | MARINE 20 | 6.15 | Mollusc fragments & benthics | 11,300 | 615 | 60 | −0.7 | 12,654 | 12,479 | 12,798 |

Ponto-Caspian basins. Three distinctive (OEG) are defined, corresponding to three main different palaeoenvironments: marine, Ponto-Caspian and coastal (*Tuberoloxoconcha*) assemblages (Table 2). The marine OEG includes typical marine Mediterranean ostracods, the Ponto-Caspian OEG includes brackish taxa from Black and Caspian seas, the coastal assemblage includes several species of *Tuberoloxoconcha*. The *Tuberoloxoconcha* genus includes interstitial, burrowing species, phytophiles or epipsammitic (living inside the surficial sandy layers), that can live in a wide range of salinities (5–34‰) in the Atlantic Ocean, as well as the Mediterranean and the Black seas (Danielopol and Bonaduce, 1990; Horne, 1989; Zenina et al., 2022). They are documented in marsh environments connected to estuaries, lagoons, fine sand intertidal areas with algae, and sandy beaches, at a maximum depth of 40 m below sea level (Cabral and Loureiro, 2013; Horne et al., 2022). *Tuberoloxoconcha* spp. Is very habitat-specific, living in athalassic and brackish coastal zones and thus is an excellent shoreline marker. The shell preservation of the marine and the *Tuberoloxoconcha* group is excellent with minimal signs of physical or chemical [dissolution] alteration. For example, fine spines on the surface of *Henryhowella* are extremely well-preserved. Juvenile and adult valves and occasional articulated carapaces are present in most samples, most notably *Tuberoloxoconcha*. The Ponto-Caspian glacial lake assemblages also contain adult and juvenile valves of most species, although those of the common genus *Candona* are often broken which is expected due to its thin, relatively fragile andlarge size shells. Fig. 3 shows the ostracode assemblages from Site M0080 used to infer environmental changes during the last deglacial sea level rise in the Gulf of Alkyonides (Supplementary Table 1).

Given the relative base level history of the Corinth-Alkyondies depocentres (Collier et al., 2000; Leeder et al., 2005) and the present water depth at Site M0080, deposition at this site during the last deglaciation would have been at about 300–310 m water depth under lacustrine conditions and up to 350 m below sea level under marine conditions. The extraordinary preservation of ostracodes implies that many of these particles may have been transported out into the basin by low concentration (hypopycnal) plumes. Paralic ostracodes may have been reworked by rivers migrating or avulsing across the lagoonal and coastal environments where they were endemic, or in low-concentration plumes generated by coastal wave action. Sediment grains and ostracods would have then settled as hemipelagic particles with few grain-to grain-abrasive

**Table 2**
Faunal zones based on ostracod assemblages.

| M80 Zones | Climate Interval[b] | M80 Core depth (cm) | Linear Age Model | Bacon Age Model | Alkyonides Gulf Environment | Faunal features | Global Sea Level [a] |
|---|---|---|---|---|---|---|---|
| Marine A | Younger Dryas-E. Holocene | 360–550 | 7929 −13146 | 8257 −12964 | Fully Mediterranean Marine | Diverse Mediterranean fauna | 14–12.5 ka - 20 m SLR in 1500 years |
| Marine B | Late Bolling-Allerod | 550–602 | 13,146 −14917 | 12,964 −14946 | Initial Intermittent marine | Alternating Mediterranean/ *Tuberoloxoconcha* spp. | Rapid SLR 13–15 ka, 40 mm/yr |
| *Tuberoloxoconcha* spp. subzone A | Bolling-Allerod | 552–600 | 13,474 −14860 | 13,032 −14890 | Initial Intermittent marine | Alternating Mediterranean/ *Tuberoloxoconcha* spp. | Rapid SLR 14.5–14 ka, MWP-1A |
| *Tuberoloxoconcha* spp. subzone B | Late Heinrich Event 1 | 600–672 | 14,860 −16881 | 14,890 −16847 | Stable brackish | Dominant Stable *Tuberoloxoconcha* spp. | 18–16.5 ka: near stable SL, short Late H-1 SLR |
| *Tuberoloxoconcha* spp. *subzone* C | Early Deglacial; Heinrich 1 | 680–790 | 17,170 −20343 | 17,318 −19748 | Intermittent brackish/lacustrine | *Tuberoloxoconcha* spp.alternating with Pont-Caspian | 19 kyr MWP[b] |
| Ponto-Caspian | Last Glacial Maximum | 682–790 | 17,227 −20346 | 17,151 −19748 | Ponto-Caspian Lake, Intermittent brackish/lacustrine | Mainly Ponto-Caspian Lake, *Candona* spp. | LGM global SL ~ -125 m |

[a] See Clark et al., 2009, Lambeck et al., (2014), Peltier et al., (2015).
[b] See Clark et al., (2012).

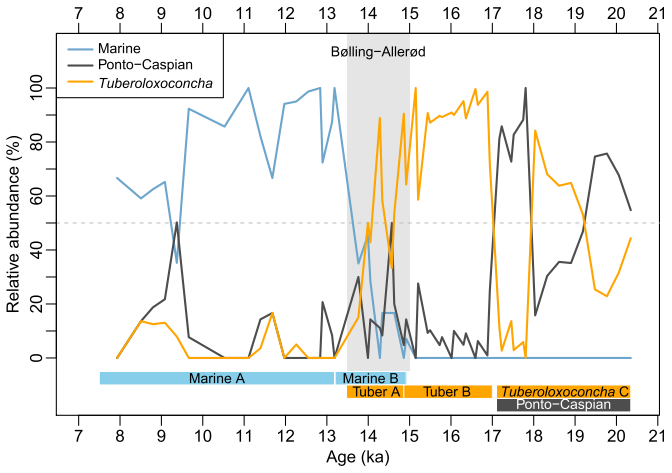


**Fig. 3.** Major ostracode faunal zones from the 8 to 3 mbsf core depth from Hole M0080A. Marine (blue), Ponto-Caspian (black), and *Tuberoloxoconcha* spp. (orange) subzones are indicators of marine, lacustrine, and brackish, saline lake environments. Six faunal zones and subzones represent a progressive transition from lacustrine to fully marine environments. *Tuberoloxoconcha* spp. Subzone C and Ponto-Caspian zones alternate with each other during ~20–17 ka and represent intermittent brackish and lacustrine environments, respectively. *Tuberoloxoconcha* spp. Subzone B is characterized by the dominance of *Tuberoloxoconcha* (80–100%) and represents a stable coastal environment ~ 17–15 ka. *Tuberoloxoconcha* spp. Subzone A and Marine subzone B partially overlap with the Bølling–Allerød warming event (14.6–12.89 ka; gray shading) and are characterized by alternating Mediterranean marine fauna and littoral brackish *Tuberoloxoconcha* species. Marine A is characterized by diverse Mediterranean marine fauna and represents a generally stable marine environment. Age model uses calibrated radiocarbon dates in Table 1 and plotted in Supplementary Fig. 1. The Bølling/Allerød interstadial interval is noted.

interactions (as opposed to being reworked by much more abrasive turbulent underflows). The active tectonic uplift of the southern coastline of the Alkyonides Gulf, at a rate of ~0.3 m/kyr (Leeder et al., 2005), may have promoted rapid erosion of coastal sediments. Bathyal species may on the other hand be preserved in situ.

### 3.3. MIS 2-1 transition during termination I

#### 3.3.1. Interval from 20.5 ka to 17 ka

The term Ponto-Caspian (Ponto-Caspian Zone, Fig. 3) has been applied to saline lake environments of the region and distinct saline-lake faunas formed in Paratethyan basins over the last 15 million years in the eastern Mediterranean. Ponto-Caspian lakes, like the modern Caspian Sea and the Black Sea prior to Holocene marine flooding, were isolated from marine influence. These types of lakes, not in connection with sea water and characterized by inhomogeneity in ionic proportions, are called athalassic (Bayly, 1969). Their ostracode fauna is highly different from that recovered in and around coastal brackish environments with marine influence (De Deckker, 1981). Ponto-Caspian lakes hosted diverse ostracode faunas, often with endemic species. Those Ponto-Caspian faunas in the Corinth-Alkyonides Gulf drill site M0080 include taxa such as *Candona*, *Amnicythere*, and certain species of *Leptocythere*, which dominated the non-marine lake phases during glacial periods.

In the Gulf of Alkyonides, dominant lacustrine and coastal assemblages characterize the glacial lake phase ~20–18.5 ka. These include lacustrine Ponto-Caspian assemblages and a distinct, coastal group, *Tuberoloxoncha* spp. The brief dominance of Ponto-Caspian assemblages at ~18–17 ka in the Alkyonides cores coincides with the well-known climate event known as Heinrich Event 1, although the climatic and environmental significance of Heinrich Event 1 in the Gulf of Alkyonides requires further study.

#### 3.3.2. Interval from 17 ka to 15 ka

In the *Tuberoloxoconcha* spp. Subzone B, this group dominates (74–99%) the Alkyonides fauna between 670 and 600 cm core depth signifying a stable coastal environment in a glacial lake between ~ 17 and 15 ka. We interpret this as a period of nearly stable hydroclimate with minimal variability in athalassic faunas. Our radiocarbon dating supports this period being slightly younger than the period of relatively stable sea level and northern hemisphere climate from approximately 18 to 16.5 ka. Importantly, near-constant paleoclimate conditions imply a slowdown of deglaciation and coincide with plateaus in the Antarctic ice core deuterium (Jouzel et al., 2007) and NGRIP Greenland ice core oxygen isotope records (Obrochta et al., 2014).

#### 3.3.3. Interval from 15 ka to 13.2 ka

*Tuberoloxoconcha* spp. Subzone A is characterized by rapidly decreasing percentages of this species and coincident increases of marine species from 0 to 100% of the assemblages (Marine subzone B). This critical period corresponds with the period of rapid

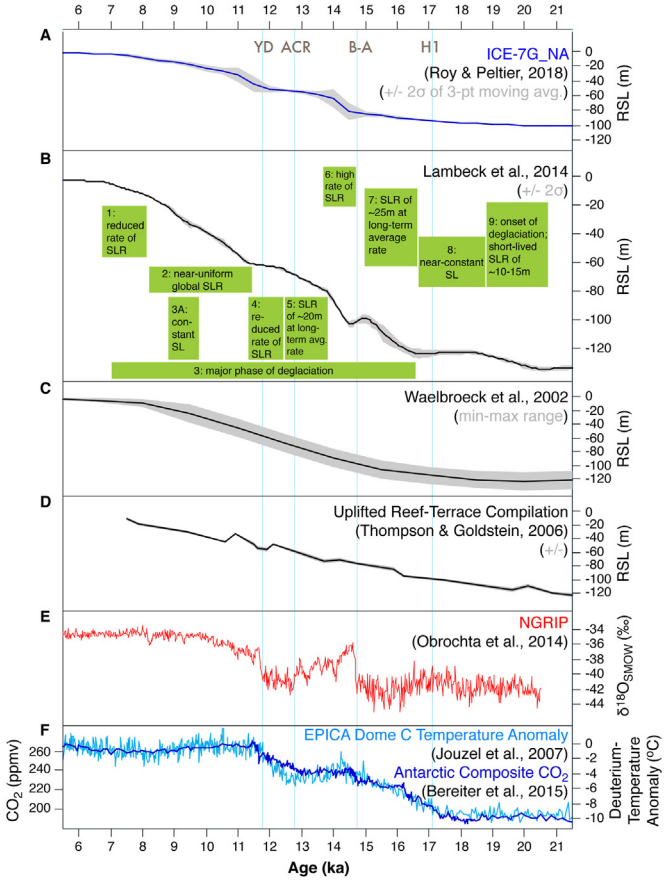


**Fig. 4.** Global sea level and climatic events during the Marine Isotope Stage (MIS) 2–1 transition. A. ICE-7G_NA regional sea level model of Roy and Peltier (2018) for the Rion and Acheloos-Cape Pappas sill region separating the Corinth-Alkyonides system from the Mediterranean. B. Global sea-level curve from Lambeck et al. (2014). Green boxes indicate stages of RSL changes (Lambeck et al., 2014). C. Global sea-level curve from Waelbroeck et al. (2002) based on dep-sea foraminiferal oxygen isotope records corrected for deep bottom water temperatures. D. Uplifted coral reef-terrace compilation sea-level record from Thompson and Goldstein (2006). North GRIP Greenland oxygen isotope record showing major northern hemisphere deglacial events (Andersen et al., 2004; Rasmussen et al., 2006; Obrochta et al., 2014). F. Deuterium-derived temperature anomaly record from EPICA Dome C ice core (light blue), Antarctica (Jouzel et al., 2007; Jouzel et al., 2001, 2007), and the Antarctic composite $CO_2$ record of Bereiter et al. (2015). Abbreviations: YD=Younger Dryas, ACR = Antarctic Cold Reversal, B-A= Bølling-Allerød, H1= Heinrich Event 1.

hemispheric warming and global sea level rise during the BØlling-AllerØd interstadial period (B-A) ~ 15–13.5 ka.

### 3.3.4. Interval from 13.2 ka to 8 ka

Finally, the marine assemblage (Marine subzone A, Fig. 3, ~13.2 to 8 ka) includes at least 27 species dominated by the genera *Henryhowella*, *Cytheropteron*, *Loxoconcha* and others typical of modern eastern Mediterranean faunas. There is variability in the most dominant marine species during the late deglacial and Holocene interglacial probably reflecting differences in water depth, bottom environments, and perhaps source Mediterranean faunas. However, we note that *Henryhowella sarsi* (Muller) is typically a bathyal species in the Mediterranean (Bonaduce et al., 1999), which suggests a paleodepth ~100–400 m, roughly similar to the modern water depth of 348 m at the core site. There is a brief increase in Ponto-Caspian species at ~10-9ka which is attributed to likely reworking from older glacial sediments.

## 4. Discussion

The Gulf of Alkyonides IODP Site M0080 allows us to examine the phases of glacial and deglacial paleoclimate and relative sea level change during Termination 1. A selection of global sea-level and paleoclimate curves during the Marine Isotope Stage (MIS) 2–1 transition are illustrated in Fig. 4. In Fig. 4A we show RSL estimates for the study region, which were determined by correcting the ESL record of Waelbroeck et al. (2002) for land elevation throughout Termination 1 predicted by the ICE-7G_NA (VM7) GIA model of Roy and Peltier (2018) and Peltier (2021). Fig. 4B through 4F show the global sea level curves from Lambeck et al. (2014, multiple coastal sources), Waelbroeck et al. (2002, oxygen isotope ice volume corrected for bottom temperatures), and Barbados (Peltier et al., 2015;2008), as well as the North Greenland Ice Core oxygen isotope (updated by Obrochta et al., 2014) and Antarctica deuterium (Jouzel et al., 2007) paleoclimate records.

The relationships between the ostracode faunal patterns and the periods of global sea level change are illustrated in Fig. 5. At the onset of deglaciation (~21–19 ka BP), there is a short-lived global sea-level rise (SLR) of ~10–15 m (Clark and Huybers, 2009; Lambeck et al., 2014), which is not seen in the continuing lacustrine environment of the Alkyonides Gulf. Subsequently, Lambeck et al. (2014) documented a ~25-m global SLR at ~16.5–15 ka BP that was the main phase of deglaciation. The Alkyonides faunas also suggest a rapid transition from saline lake to fully marine environments beginning about 15 ka and accelerating until 13.5 ka. This sea-level rise coincides with the BØlling-AllerØd interstadial period (B-A), an abrupt northern hemisphere warming event during the deglaciation, corresponding with Meltwater Pulse 1 A. This faunal shift from non-marine and coastal species to near 100% marine ostracode species in the Alkyonides record (Marine-Mediterranean fauna, Figs. 3 and 5) thus appears to be coincident with the abrupt hemispheric-wide B-A warming identified in many paleoclimate records (Fig. 4). This transition represents the most rapid global SLR rate of the last deglaciation, lasting about 500 years, and it is most likely that the B-A sea-level rise event in the Gulf of Alkyonides resulted in the full breaching of the Rion and Acheloos-Cape Pappas sills at the western entrance to the Gulf of Corinth and hence the Gulf of Alkyonides (Fig. 5).

Lambeck et al. (2014) estimated a total SLR of ~20 m from ~14 to ~12.5 ka BP, a ~1500-year period when marine species dominate the Site M0080 record. A reduced rate of SLR from ~12.5–11.5 ka BP, near-uniform global SLR from ~11.4 to 8.2 ka BP, and reduced SLR

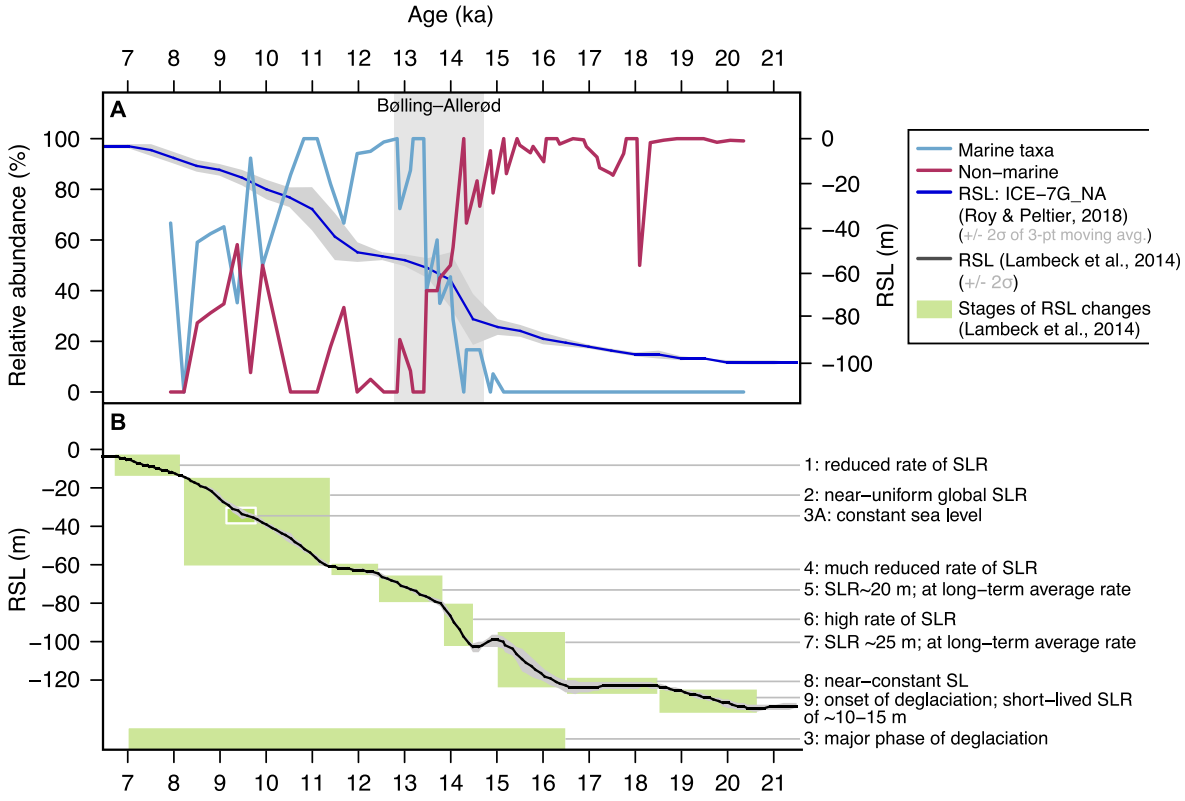


**Fig. 5.** A. M0080 faunal zones with characteristic Alkyonides Gulf paleoenvironments (Table 2) plotted against ICE-7G_NA regional sea level curve. B. Global sea-level curve from Lambeck et al. (2014) with global sea-level trends identified throughout the deglacial interval.

rate from 8.2 to 6.7 ka BP do not appear to be reflected in the ostracode faunas as the Corinth-Alkyonides Gulf system had already become fully marine.

## 5. Conclusions

The non-marine to marine transition in Alkyonides ostracode assemblages centered on 15–13.5 ka demonstrates that, despite the active tectonic setting, the primary forcing of sedimentation and paleoenvironments in the Gulf of Alkyonides is global glacio-eustatic sea level cycles driven by global ice volume. As with deep-sea isotope records of glacial terminations, intervals of deglaciation were extremely abrupt, occurring over 1–3 m of core section. These results confirm interpretations of multiple previous studies (e.g., Nixon et al., 2016; references therein) that Alkyonides seismic stratigraphy reflects mid to late Quaternary sea-level oscillations.

Due to the high sedimentation rate, the Alkyonides paleo-sea level record provides a unique test of global sea-level records from geophysical models and reveals new details about the last deglaciation. These include:

1. Fluctuating non-marine, saline lake environments from ~20 ka to 15 ka, with a possible signal for Heinrich Event 1 near ~18–17 ka;
2. A ~500–1000 year period of stable lacustrine environments ~16.5 to 15.5 ka, slightly younger than the stable climate shown in the sea level record of Lambeck et al. (2014) and coincident with plateaus in Antarctic and Greenland paleoclimate curves;
3. The well-known large (~20 m), rapid (<500 years), SLR during the Bølling–Allerød interstadial centered on ~14.5 ka corresponding with Meltwater Pulse (MWP) 1 A;
4. Complete flooding of the Alkyonides Gulf by the Younger Dryas and early Holocene including the post-YD MWP 1 B (13.3–10 ka).

## Credit author statement

**Ilaria Mazzini**: Conceptualization, Formal analysis, Investigation, writing -original draft, Validation, Supervision. **Thomas M. Cronin**: Conceptualization, Formal analysis, Investigation, writing -original draft, Validation, Supervision. **Lisa C. McNeill**: Supervision. **Donna J. Shillington**: Supervision. **Robert L. Gawthorpe**: writing-review & editing, Validation. **Richard E. Ll. Collier**: writing-review & editing, Validation. **Gino de Gelder**: formal analysis. **Anna Rose Golub**: Investigation. **Michael R. Toomey**: Investigation, Formal analysis. **Robert K. Poirie**r: Investigation, Formal analysis. **Huai-Hsuan May Huang**: investigation, Formal analysis, Visualization. **Marcie Purkey Phillips**: investigation, Formal analysis.

## Declaration of competing interest

The authors declare that they have no known competing financial interests or personal relationships that could have appeared to influence the work reported in this paper.

## Data availability

All data are provided in the supplementary material

## Acknowledgments

We are grateful to the shipboard scientific staff and crew of the *Fugro Synergy*, mission-specific platform, for the initial work on IODP 381 Site M0080 and Holger Kuhlmann and the Bremen, Germany IODP repository for assistance in sampling the core. IM was funded by the CNR-Short Term Mobility Program 2018 and TMC, ARG, RP, and MRT by the USGS Climate Research & Development Program. Any use of trade, firm, or product names is for descriptive purposes only and does not imply endorsement by the U.S. Government.

## Appendix A. Supplementary data

Supplementary data to this article can be found online at https://doi.org/10.1016/j.quascirev.2023.108192.

## References

Andersen, K., Azuma, N., Barnola, J.M., Bigler, M., Biscaye, P., Caillon, N., Chappellaz, J., Clausen, H., Dahl-Jensen, D., Fischer, H., Flückiger, J., Fritzsche, D., Fujii, Y., Goto-Azuma, K., Grønvold, K., Gundestrup, N., Hansson, M., Huber, C., Hvidberg, C., White, J., 2004. High-resolution record of Northern Hemisphere climate extending into the last interglacial period. Nature 431, 147–151. https://doi.org/10.1038/nature02805.

Bayly, I.A.E., 1969. Symposium on 'salt and brackish inland waters'. Introductory Comments. Verh. Int. Ver. Limnol. 17, 419–420.

Bereiter, B., Eggleston, S., Schmitt, J., Nehrbass-Ahles, C., Stocker, T.F., Fischer, H., Kipfstuhl, S., Chappellaz, Je, 2015. Revision of the EPICA Dome C CO2 record from 800 to 600 kyr before present. Geophys. Res. Lett. 42 (2). https://doi.org/10.1002/2014GL061957.

Blaauw, M., Christen, J.A., 2011. Flexible paleoclimate age-depth models using an autoregressive gamma process. Bayesian Analysis 6, 457–474.

Bonaduce, G., Barra, D., Aiello, G., 1999. The genus Henryhowella Puri, 1957 (Crustacea, Ostracoda) in the Atlantic and Mediterranean from Miocene to Recent. Bollettino della Società Paleontologica Italiana 38, 59–72.

Cabral, M.C., Loureiro, I.M., 2013. Overview of Recent and Holocene ostracods (Crustacea) from brackish and marine environments of Portugal. J. Micropalaeontol. 32, 135–159. https://doi.org/10.1144/jmpaleo2012-019.

CALIB rev. 8; Stuiver, M., Reimer, P.J., 1993, Radiocarbon, 35, 215-230.

Clark P.U., Dyke A. S., Shakun J.D., Carlson A.E., Clark J., Wohlfarth B., Mitrovica J.X., Hostetler, S.W, McCabe, A.M. 2009. The Last Glacial Maximum. Science (New York, N.Y.). 325: 710-4. PMID 19661421 DOI: 10.1126/Science.1172873.

Clark, P.U., Huybers, P., 2009. Interglacial and future sea level. Nature 462 (7275), 856–857. https://doi.org/10.1038/462856a.

Clark, J., McCabe, A.M., Bowen, D.Q., Clark, P.U., 2012. Response of the Irish Ice Sheet to abrupt climate change during the last deglaciation. Quaternary Science Reviews 35, 100–115.

Collier, R.E., Leeder, M.R., Trout, M., Ferentinos, G., Lyberis, E., Papatheodorou, G., 2000. High sediment yields and cool, wet winters: test of last glacial paleoclimates in the northern Mediterranean. Geology 28 (11), 999–1002. https://doi.org/10.1130/0091-7613(2000)28<999:HSYACW>2.0.CO;2.

Danielopol, D.L., Bonaduce, G., 1990. The colonization of subsurface habitats by the loxoconchidae sars and psammocytheridae klie. In: Whatley, R., Maybury, C. (Eds.), Ostracoda and Global Events. Chapman and Hall, London, pp. 437–458.

De Deckker, P., 1981. Ostracods of athalassic saline lakes. A review. Hydrobiologia 81, 131–144.

de Gelder, G., Fernández-Blanco, D., Melnick, D., et al., 2019. Lithospheric flexure and rheology determined by climate cycle markers in the Corinth Rift. Sci Rep 9, 4260. https://doi.org/10.1038/s41598-018-36377-1.

Elderfield, H., Ferretti, P., Greaves, M., Crowhurst, S., McCave, I.N., Hodell, D., Piotrowski, A.M., 2012. Evolution of ocean temperature and ice volume through the mid-pleistocene climate transition. Science 337 (6095), 704–709. https://doi.org/10.1126/science.1221294.

Horne, D.J., 1989. On *Tuberoloxoconcha atlantica* Horne sp. nov. Stereo-Atlas Ostracod Shells 16 (17), 73–76.

Horne, D.J., Cabral, M.C., Fatela, F., Radl, M., 2022. Salt marsh ostracods on European Atlantic and North Sea coasts: aspects of macroecology, palaeoecology, biogeography, macroevolution and conservation. Mar. Micropaleontol. 174, 101975. https://doi.org/10.1016/j.marmicro.2021.101975.

Jouzel, J., Masson, V., Cattani, O., Falourd, S., Stievenard, M., Stenni, B., Longinelli, A., Johnsen, S.J., Steffenssen, J.P., Petit, J.R., Schwander, J., Souchez, R., Barkov, N.I., 2001. A new 27 ky high resolution East Antarctic climate record. Geophysical Research Letters 28. https://doi.org/10.1029/2000GL012243.

Jouzel, J., Masson-Delmotte, V., Cattani, O., Dreyfus, G., Falourd, S., Hoffmann, G., Minster, B., Nouet, J., Barnola, J.M., Chappellaz, J., Fischer, H., Gallet, J.C., Johnsen, S., Leuenberger, M., Loulergue, L., Luethi, D., Oerter, H., Parrenin, F., Raisbeck, G., Raynaud, D., Schilt, A., Schwander, J., Selmo, E., Souchez, R., Spahni, R., Stauffer, B., Steffensen, J.P., Stenni, B., Stocker, T.F., Tison, J.L., Werner, M., Wolff, E.W., 2007. Orbital and millennial antarctic climate variability over the past 800,000 years. Science 317 (5839), 793–797. https://doi.org/10.1126/science.1141038.

Konijnendijk, T.Y.M., Ziegler, M., Lourens, L.J., 2015. On the timing and forcing

mechanisms of late Pleistocene glacial terminations: insights from a new high-resolution benthic stable oxygen isotope record of the eastern Mediterranean. Quat. Sci. Rev. 129, 308–320. https://doi.org/10.1016/j.quascirev.2015.10.005.
Lambeck, K., Rouby, H., Purcell, A., Sun, Y., Sambridge, M., 2014. Sea level and global ice volumes from the last glacial maximum to the Holocene. Proc. Natl. Acad. Sci. USA 111 (43), 15296–15303. https://doi.org/10.1073/pnas.1411762111.
Lea, D.W., Martin, P.A., Pak, D.K., Spero, H.J., 2002. Reconstructing a 350 ky history of sea level using planktonic Mg/Ca and oxygen isotope records from a Cocos Ridge core. Quat. Sci. Rev. 21, 283–293. https://doi.org/10.1016/S0277-3791(01)00081-6.
Leeder, M.R., Collier, R.L., Aziz, L.A., Trout, M., Ferentinos, G., Papatheodorou, G., Lyberis, E., 2002. Tectono-sedimentary processes along an active marine/lacustrine half-graben margin: Alkyonides Gulf, E. Gulf of Corinth, Greece. Basin Res. 14 (1), 25–41. https://doi.org/10.1046/j.1365-2117.2002.00164.x.
Leeder, M.R., Portman, C., Andrews, J.E., Collier, R.E.Ll, Finch, E., Gawthorpe, R.L., McNeill, L.C., Perez-Arlucea, M., Rowe, P., 2005. Normal faulting and crustal deformation, Alkyonides Gulf and Perachora peninsula, eastern Gulf of Corinth rift basin, Greece. Journal of the Geological Society, London 162, 549–561. https://doi.org/10.1144/0016-764904-075.
Lisiecki, L.E., Raymo, M.E., 2005. A Pliocene-Pleistocene stack of 57 globally distributed benthic *18O records. Paleoceanography 20, PA1003. https://doi.org/10.1029/2004PA001071.
Lisiecki, L.E., Raymo, M.E., 2009. Diachronous benthic d18O responses during late Pleistocene terminations. Paleoceanography 24, PA3210. https://doi.org/10.1029/2009PA001732.
Mazzini, I., Rossi, V., Da Prato, S., Ruscito, V., 2017. Ostracods in archaeological sites along the Mediterranean coastlines: three case studies from the Italian peninsula. In: Williams, M., Hill, T., Boomer, I., Wilkinson, I.P. (Eds.), 2017. The Archaeological and Forensic Applications of Microfossils: A Deeper Understanding of Human History. The Micropalaeontological Society, Special Publications. Geological Society, London, pp. 121–142.
McNeill, L.C., Shillington, D.J., Carter, G.D.O., the Expedition 381 Participants, 2019a. Corinth active rift development. In: Proceedings of the Inter- National Ocean Discovery Program, 381: College Station, TX (International Ocean Discovery Program). https://doi.org/10.14379/iodp.proc.381.2019.
McNeill, L.C., Shillington, D.J., Carter, G.D.O., Everest, J.D., Gawthorpe, R.L., Miller, C., Phillips, M.P., et al., 2019b. High-resolution record reveals climate-driven environmental and sedimentary changes in an active rift. Sci. Rep. 9, 3116. https://doi.org/10.1038/s41598-019-40022-w.
Nixon, C.W., McNeill,L.C., Bull, J.M. Bell,R.E., Gawthorpe,R.L., Henstock, T.J., Christodoulou,D. , Ford, M., Taylor, B., Sakellariou, D., Ferentinos, G., 2016. Rapid spatiotemporal variations in rift structure during development of the Corinth Rift, Central GreeceTectonics, 35 (5) 1225-1248, 10.1002/2015TC004026.
Obrochta, S.P., Yokoyama, Y., Moren, J., Crowley, T.J., 2014. Conversion of GISP2-based sediment core age models to the GICC05 extended chronology. Quat. Geochronol. 20, 1–7. https://doi.org/10.1016/j.quageo.2013.09.001.
Past Interglacials Working Group of PAGES, 2016. Interglacials of the last 800,000 years. Rev. Geophys. 54, 162–219. https://doi.org/10.1002/2015RG000482.
Peltier, W.R., Argus, D.F., Drummond, R., 2015. Space geodesy constrains ice age terminal deglaciation: the global ICE-6G_C (VM5a) model. J. Geophys. Res. Solid Earth 120, 450–487. https://doi.org/10.1002/2014JB011176.
Peltier, W.R., 2021. https://www.atmosp.physics.utoronto.ca/~peltier/data.php.
Rasmussen, S.O., Andersen, K.K., Svensson, Anders M., Steffensen, Jørgen Peder, Vinther, Bo Møllesøe, Clausen, Henrik Brink, Siggaard-Andersen, Marie-Louise, Johnsen, Sigfús Jóhann, Larsen, L.B., Dahl-Jensen, Dorthe, Bigler, Matthias, Röthlisberger, Regine, Fischer, Hubertus, Goto-Azuma, Kumiko, Hansson, Margareta E., Ruth, Urs, 2006. A new Greenland ice core chronology for the last glacial termination. J. Geophys. Res. Atmos. 111, D06102. https://doi.org/10.1594/PANGAEA.586838.
Reimer, P., et al., 2020. The IntCal20 northern hemisphere radiocarbon age calibration curve (0–55 cal kBP). Radiocarbon 62 (4), 725–757. https://doi.org/10.1017/RDC.2020.41.
Roy, K., Peltier, W.R., 2018. Relative sea level in the Western Mediterranean basin: a regional test of the ICE-7G_NA (VM7) model and a constraint on Late Holocene Antarctic deglaciation. Quat. Sci. Rev. 183, 76–87. https://doi.org/10.1016/j.quascirev.2017.12.021.
Stuiver, M., Reimer, P.J., Reimer, R.W., 2021. CALIB 8.2 [WWW program] at. http://calib.org.
Taylor, B., Weiss, J.R., Goodliffe, A.M., Sachpazi, M., Lai-Gle, M., Hirn, A., 2011. The structures, stratigraphy andevolution of the Gulf of Corinth rift, Greece. Geophys. J. Int.,185,, 1189–1219.
Thompson, W.G., Goldstein, S.L., 2006. A radiometric calibration of the SPECMAP timescale. Quat. Sci. Rev. 25, 3207–3215. https://doi.org/10.1016/j.quascirev.2006.02.007.
Waelbroeck, C., Labeyrie, L., Michel, E., Duplessy, J.C., McManus, J.F., Lambeck, K., Balbon, E., Labracherie, M., 2002. Sea-level and deep water temperature changes derived from benthic foraminifera isotopic records. Quat. Sci. Rev. 21, 295–305. https://doi.org/10.1016/S0277-3791(01)00101-9.
Zenina, M.A., Kolyuchkina, G.A., Murdmaa, I.O., Aliev, R., Borisov, D.G., Dorokhova, E.V., Zatsepin, A.G., 2022. Ostracod assemblages from the Golubaya (Rybatskaya) Bay area on the outer northeastern Black Sea shelf over the last 300 years. Mar. Micropaleontol. 174, 102129. https://doi.org/10.1016/j.marmicro.2022.102129.